Comparative Evaluation of an ISAC Precoding Scheme for OTFS and OFDM Waveforms in Perceptual Mobile Networks

Ali Göktas*, Mikko Valkama*, Bo Tan†*

*Tampere Wireless Research Centre, Faculty of Information Technology and Communication Sciences, Tampere University, Tampere, Finland, {ali.goktas, mikko.valkama, bo.tan}@tuni.fi

† Department of Eletronics and Electrical Engineering, University College London, tan.bo@ucl.ac.uk

***Abstract*—The popularization of the perceptual mobile networks (PMN) concept gives rise to the waveform design for integrated sensing and communications (ISAC). In this work, we propose a precoding scheme for ISAC, which is applicable for either orthogonal time frequency space (OTFS) and orthogonal frequency-division multiplexing (OFDM) waveforms, the two most discussed waveforms in B5G or 6G PMNs. The essence of the precoding scheme is shaping the envelope of the specific communication symbols according to the expected reference sensing signal, which is derived from point targets and is associated with the time-frequency (TF) or delay-Doppler (DD) grids in OFDM or OTFS blocks/frames, respectively. The proposed precoder provides an adaptive adjustment mechanism between the sensing and communications functions for diverse applications in the PMN. We conduct simulations to demonstrate the trade-off between communications and sensing performances in terms of bit error rate (BER) and detection probability, respectively. The simulation results reveal that the OFDM-based ISAC waveform shows greater robustness on retaining the communication performance than the OTFS-based approach when the system has to lean towards the sensing function. We also identify the potential reason for this observation as the effective channel in OTFS case being spread more widely along the time domain, which gives the precoder fewer degrees of freedom when optimizing the transmit waveform.**

***Index Terms*—ISAC, delay-Doppler, OFDM, OTFS, precoding, convex optimization.**

I. Introduction

THE extension and diversification of the mobile services and application scenarios such as supporting autonomous vehicles, smart healthcare and factories, drove the mobile networks towards multifunctional evolution in the past few years. Transceiving information symbols is no longer the only function of mobile networks. Integrating the radio sensing function in the data-carrying signal is considered essential to support the new applications. The radio networks with the capability of detecting, estimating, and modeling the surrounding objects and environment are called perceptual mobile networks (PMN), which is underpinned by the evolving technology of integrated sensing and communications (ISAC). Research works on ISAC in the context of 5G and 6G mobile networks have been emerging [1], [2] due to its importance in enabling the new mobile applications.

A primary challenge in ISAC research is designing the waveform that achieves two objectives: effective information transmission and precise signal detection and estimation. The former objective (communications) results in a waveform with high randomness, while the second objective (sensing) requires determinism in the waveforms [3].

To integrate two conflicting requirements in one waveform, researchers have explored approaches that allocate the communications and sensing functions to the orthogonal time, frequency, or spatial domain resource blocks. It has been shown in [4] that time division duplex (TDD) based packet communication could be modified to reuse the TDD frame structure by integrating the sensing function to the system. Likewise, sensing functionality is seamlessly integrated into a vehicular communication system in [5] by utilizing the pilot signals which are multiplexed in the frequency domain with communication function. The optimal beamforming design described in [6] is an example of spatially multiplexing the sensing and communication functionalities by creating a suitable antenna pattern. Orthogonal time frequency space (OTFS) signal, which multiplexes information symbols in the 2D delay-Doppler (DD) domain for high mobility communications design, also provides the extended dimensions for resource allocation between communications and sensing functions [7]. So far, the research community is still unfolding the potential of OTFS-based the ISAC waveform design.

We propose a precoding scheme for OTFS-based ISAC waveform design in this work, which reshapes the OTFS communication signal towards a predefined reference sensing signal that is acquired from prior sensing interactions [8]. The reshaped OTFS signal not only contains the original modulated information, but is also favorable for performing sensing functions (e.g., detection and estimation). The proposed precoding scheme presents three notable features: 1). Encoding the sensing function into the OTFS signal without losing the information rate; 2). providing a parameter ρ to adaptively control the degree of waveform reshaping; 3). wide-ranging applicability on the other waveforms, particularly OFDM.

II. Signal Models of OTFS and OFDM

We consider a single-input single-output (SISO) system that utilizes a waveform which carries communication messages and will be reshaped by a precoder $\boldsymbol{W}$ to be more favorable for performing sensing functions (e.g., detection or estimation). An overview of the process is shown in Fig. 1 where the

This work is part of the European Union's MSCA RISE programme DIOR project (under grant agreement 10100828), and Academy of Finland ACCESS project (339519).

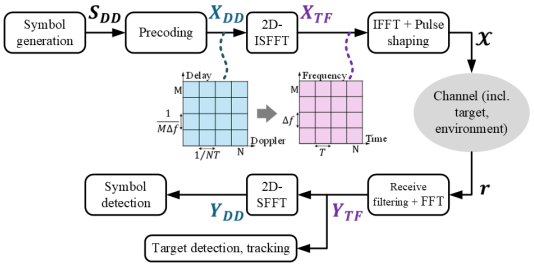

Fig. 1. Input-output relationship of the proposed OTFS system visualized as a diagram.

starting point is an $M \times N$ block of the communication message. M is number of time delay bins and N is number of Doppler shift bins. The resolution is $\frac{1}{M\Delta f}$ for one delay tap and $\frac{1}{NT}$ for one Doppler tap, with Δf and T being the subcarrier spacing of the OTFS samples and symbol duration in the time-frequency (TF) domain, respectively. Message is assumed to consist of quadrature phase shift keying (QPSK) symbols in this work, although any order of PSK is suitable for the same model. The channel state information (CSI) is assumed to be known in this section, and is considered to be estimated in the receiver side by the DD channel estimation methods described in [8].

Let us represent the uncoded QPSK symbols in DD domain as $\boldsymbol{S}_{DD} \in \mathbb{C}^{M\times N}$, and define the preceded symbols as

$$\boldsymbol{X}_{DD} = \boldsymbol{S}_{DD} \odot \boldsymbol{W}_{DD}, \tag{1}$$

with $\boldsymbol{W}_{DD}$ being the matrix of precoding weights that are applied to $\boldsymbol{S}_{DD}$ via element-wise multiplication. The channel between the base station (BS) and user equipment (UE) is given in DD domain by

$$h_{DD}(\tau,\nu) = \sum_{i=0}^{P} h_i \delta(\tau-\tau_i)\delta(\nu-\nu_i), \tag{2}$$

where $\tau_i \in [0, \tau_{max}]$ is the delay along the i-th path, $\nu_i \in [-\nu_{max}, \nu_{max}]$ is the Doppler shift along the i-th path, $h_i \in \mathbb{C}$ is the channel coefficient of the i-th path, and $P \in \mathbb{Z}^+$ is the number of multipaths between the BS and UE. Delay and Doppler taps in terms of τ and ν values are $\ell_i = \tau_i M\Delta f \in \mathbb{R}$ and $\kappa_i = \nu_i NT \in \mathbb{R}$, where $\ell \in \mathcal{L}$ and $\kappa \in \mathcal{K}$ are the sets of fractional time delay and Doppler shift indices, respectively.

The input-output characteristics of DD channels may be represented with a practical model, provided that transmit and receive filters are rectangular functions, and indices for time delays and Doppler shifts are integers. Fractional part of the elements of $\mathcal{L}$ and $\mathcal{K}$ can be eliminated by rounding them, with the sets $L = \{\text{round}(\ell_i) | i = \mathbb{Z}^+, 1 \le i \le P\}$ and $K = \{\text{round}(\kappa_i) | i = \mathbb{Z}^+, 1 \le i \le P\}$ containing the integer indices. Even though delay and Doppler shift bins being restricted as integers limit the resolution of channel path parameters, this disadvantage could be mitigated by fractional parameter estimation methods [9], [10].

The channel impulse function (2) may be represented within the delay-time domain as follows in discrete time and in baseband frequency, with the assumption that the channel delay shifts are integers [11]:

$$g^s(l,q) = \sum_{k\in K_l} \nu_l(k) z^{k(q-l)}, \tag{3}$$

where for each integer delay tap l, where q is the sample index in the delay-time channel, $K_l = \{k_i | l = l_i\}$ is the set of all rounded Doppler shift indices that correspond to the rounded time delay index of l_i, $z = e^{\frac{j2\pi}{NM}}$, and the Doppler response function $\nu_l(k)$ is defined as

$$\nu_l(k) = \begin{cases} h_i, & \text{if } l = l_i \text{ and } k = k_i, \\ 0, & \text{otherwise.} \end{cases} \tag{4}$$

Values of $g^s(l,q)$ can be represented as a matrix $\boldsymbol{g}^s \in \mathbb{C}^{l_{max}\times MN}$, where l_{max} is the rounded index that corresponds to the time delay value of τ_{max}.

Representing the channel information in $\boldsymbol{g}^s$ as a time domain channel matrix $\boldsymbol{H} \in \mathbb{C}^{MN\times MN}$, input-output relationship of the transmit signal $\boldsymbol{x} \in \mathbb{C}^{MN\times 1}$ and receive signal $\boldsymbol{r} \in \mathbb{C}^{MN\times 1}$ can be written as

$$\boldsymbol{r} = \boldsymbol{H}\boldsymbol{x} + \boldsymbol{z}, \tag{5}$$

where $\boldsymbol{z} \in \mathbb{C}^{MN\times 1}$ is the additive white Gaussian noise (AWGN). Let $\boldsymbol{H} = diag(\boldsymbol{H}_1, \boldsymbol{H}_2, \ldots, \boldsymbol{H}_N)$ where $\boldsymbol{H}_n \in \mathbb{C}^{M\times M}$ and $H_n(m, m-l) = g^s(l, M(n-1)+m)$. Representing $\boldsymbol{x}$, $\boldsymbol{r}$, and $\boldsymbol{z}$ likewise in terms of $M \times 1$ sub-vectors $\boldsymbol{x} = \left[(\boldsymbol{x}_1^T, \boldsymbol{x}_2^T, \ldots, \boldsymbol{x}_N^T)\right]^T$, $\boldsymbol{r} = \left[(\boldsymbol{r}_1^T, \boldsymbol{r}_2^T, \ldots, \boldsymbol{r}_N^T)\right]^T$, and $\boldsymbol{z} = \left[(\boldsymbol{z}_1^T, \boldsymbol{z}_2^T, \ldots, \boldsymbol{z}_N^T)\right]^T$, the input-output relationship for each block can be written as $\boldsymbol{r}_n = \boldsymbol{H}_n\boldsymbol{x}_n + \boldsymbol{z}_n$, which is shown in the matrix form as follows:

$$\begin{bmatrix} \boldsymbol{r}_1 \\ \boldsymbol{r}_2 \\ \vdots \\ \boldsymbol{r}_N \end{bmatrix} = \begin{bmatrix} \boldsymbol{H}_1 & \boldsymbol{0} & \ldots & \boldsymbol{0} \\ \boldsymbol{0} & \boldsymbol{H}_2 & \ldots & \boldsymbol{0} \\ \vdots & \vdots & \ddots & \vdots \\ \boldsymbol{0} & \boldsymbol{0} & \ldots & \boldsymbol{H}_N \end{bmatrix} \begin{bmatrix} \boldsymbol{x}_1 \\ \boldsymbol{x}_2 \\ \vdots \\ \boldsymbol{x}_N \end{bmatrix} + \begin{bmatrix} \boldsymbol{z}_1 \\ \boldsymbol{z}_2 \\ \vdots \\ \boldsymbol{z}_N \end{bmatrix}. \tag{6}$$

This effectively means that each sample in $\boldsymbol{r}_n$ is calculated as

$$r_n(m) = \sum_{l_i=0}^{l_{max}} H_n(m, m-l_i) s_n(m-l_i), \tag{7}$$

which should be interpreted as each sample in the received signal is the sum of l_{max} samples weighted with respect to the Doppler shifts and channel attenuations of paths that correspond to different delay taps.

OTFS modulation based on 2D inverse symplectic finite Fourier transform (ISFFT) is conventionally applied in digital systems as

$$\begin{aligned} \boldsymbol{X}_{OTFS} &= \boldsymbol{G}_{tx}\boldsymbol{F}_M^H(\boldsymbol{F}_M\boldsymbol{X}_{DD}\boldsymbol{F}_N^H) \\ &= \boldsymbol{G}_{tx}\boldsymbol{X}_{DD}\boldsymbol{F}_N^H, \end{aligned} \tag{8}$$

where $\boldsymbol{G}_{tx} \in \mathbb{C}^{M\times M}$ is a diagonal matrix that has samples of the pulse-shaping waveform on its diagonal, and $\boldsymbol{F}_K \in \mathbb{C}^{K\times K}$ represents a $K \times K$ discrete Fourier transform (DFT) matrix. $\boldsymbol{G}_{tx}$ is simply represented as an identity matrix when transmit pulses are rectangular, and $\boldsymbol{G}_{tx} = \boldsymbol{G}_{rx}^*$ when transmit and receive filtering uses the same waveform, which are the assumed cases in this work. An equivalent operation to (8) is defined for the column-wise vectorized expression $\boldsymbol{x}_{OTFS} = \text{vec}(\boldsymbol{X}_{OTFS})$ as [12]

$$\boldsymbol{x}_{OTFS} = (\boldsymbol{F}_N^H \otimes \boldsymbol{G}_{tx})\boldsymbol{x}_{DD}. \tag{9}$$

While (9) expresses a vector of time domain samples in terms of precoded DD domain symbols, the same operation could be done for OFDM symbols in TF domain. The process is almost the same except the 2D ISFFT/SFFT blocks in Fig. 1 are removed. TF equivalent of (1) is

$$\boldsymbol{X}_{TF} = \boldsymbol{S}_{TF} \odot \boldsymbol{W}_{TF}, \tag{10}$$

where $\boldsymbol{S}_{TF} \in \mathbb{C}^{M\times N}$ contains the QPSK symbols in TF domain over M subcarriers and N frames, $\boldsymbol{X}_{TF}$ and $\boldsymbol{W}_{TF}$ are the matrices of precoded OFDM symbols and precoding coefficients, respectively. QPSK symbol matrices from this point onward will be expressed as $\boldsymbol{S}$ regardless of in which domain they were generated in, since $\boldsymbol{S}_{DD} = \boldsymbol{S}_{TF}$ in terms of numerical values. OFDM modulation is performed on $\boldsymbol{X}_{TF}$ and $\boldsymbol{x}_{TF} = \text{vec}(\boldsymbol{X}_{TF})$ analogously to (8) and (9) as

$$\boldsymbol{X}_{OFDM} = \boldsymbol{G}_{tx}\boldsymbol{F}_M^H\boldsymbol{X}_{TF}, \text{ and,} \tag{11}$$

$$\boldsymbol{x}_{OFDM} = (\boldsymbol{G}_{tx} \otimes \boldsymbol{F}_M^H)\boldsymbol{x}_{TF}. \tag{12}$$

Cyclic prefixes (CP) are appended to $\boldsymbol{x}_{OTFS}$ and $\boldsymbol{x}_{OFDM}$ before transmission. The details of CP in the transmitting signals will be elaborated in the section III-C, while CP will be ignored when defining the input-output relation of the system since it will be removed at the receiver side nevertheless.

Input-output relationship between the transmitted and received OTFS and OFDM symbols are

$$\boldsymbol{y}_{DD} = (\boldsymbol{F}_N \otimes \boldsymbol{G}_{rx})\boldsymbol{H}(\boldsymbol{F}_N^H \otimes \boldsymbol{G}_{tx})\boldsymbol{x}_{DD} + (\boldsymbol{F}_N \otimes \boldsymbol{G}_{rx})\boldsymbol{z}, \tag{13}$$

$$\boldsymbol{y}_{TF} = (\boldsymbol{G}_{rx} \otimes \boldsymbol{F}_M)\boldsymbol{H}(\boldsymbol{G}_{tx} \otimes \boldsymbol{F}_M^H)\boldsymbol{x}_{TF} + (\boldsymbol{G}_{rx} \otimes \boldsymbol{F}_M)\boldsymbol{z}, \tag{14}$$

respectively. The time-domain transmit signal $\boldsymbol{x}$ in (5) is equal to $\boldsymbol{x}_{OTFS}$ or $\boldsymbol{x}_{OFDM}$ depending on the context, while the receive signal $\boldsymbol{r}$ relates to the received symbol vector as $\boldsymbol{y}_{DD} = (\boldsymbol{F}_N \otimes \boldsymbol{G}_{rx})\boldsymbol{r}$ for the OTFS case and as $\boldsymbol{y}_{TF} = (\boldsymbol{G}_{rx} \otimes \boldsymbol{F}_M)\boldsymbol{r}$ for the OFDM case. Reformulating the operations that relate the input symbols $\boldsymbol{x}_{DD}$ and $\boldsymbol{x}_{TF}$ to the output symbols $\boldsymbol{y}_{DD}$ and $\boldsymbol{y}_{TF}$, respectively, as an effective channel expression lets us write the (13) and (14) in the compact forms of

$$\boldsymbol{y}_{DD} = \boldsymbol{H}_{eff,OTFS}\boldsymbol{x}_{DD} + \boldsymbol{w}_{OTFS}, \text{ and} \tag{15}$$

$$\boldsymbol{y}_{TF} = \boldsymbol{H}_{eff,OFDM}\boldsymbol{x}_{TF} + \boldsymbol{w}_{OFDM}, \tag{16}$$

where $H_{eff,OTFS} \triangleq (\boldsymbol{F}_N \otimes \boldsymbol{G}_{rx})\boldsymbol{H}(\boldsymbol{F}_N^H \otimes \boldsymbol{G}_{tx})$ and $H_{eff,OFDM} \triangleq (\boldsymbol{G}_{rx} \otimes \boldsymbol{F}_M)\boldsymbol{H}(\boldsymbol{G}_{tx} \otimes \boldsymbol{F}_M^H)$, while $\boldsymbol{w}_{OTFS} \triangleq (\boldsymbol{F}_N \otimes \boldsymbol{G}_{rx})\boldsymbol{z}$ and $\boldsymbol{w}_{OFDM} \triangleq (\boldsymbol{G}_{rx} \otimes \boldsymbol{F}_M)\boldsymbol{z}$ in (15) and (16).

III. Proposed Precoding Scheme

We propose a reference signal design method that is applicable for both DD and TF domains in this section. By minimizing the element-wise Euclidean distance with the reference signal which is optimized for the sensing performance, the designated radio signal will able to convey coded information while presenting a favorable envelope for radar performance. Similar approaches can also be found in the literature [13]. Elements of the QPSK symbol matrix $\boldsymbol{S}$ will be indexed according to the subcarrier and time slots, or the delay and Doppler bins they are coded in, for OFDM and OTFS cases respectively.

A. Precoding Design

The precoding approach that we propose is based on a reference signal $\boldsymbol{S}_{ref}$ in the matrix form, defined as

$$S_{ref,mn} = \begin{cases} \rho S_{mn} D_{mn} & \text{if } D_{mn} \neq 0, \\ S_{mn} & \text{otherwise,} \end{cases} \tag{17}$$

where S_{mn} is the QPSK symbol coded into the m-th delay and n-th Doppler bin for OTFS signal, or m-th subcarrier and n-th time slot for the OFDM signal. scaling matrix $\boldsymbol{D}$ represents the different reflectivities of sensing targets, and ρ is a parameter to allocate more weight to the communication operation when it is smaller, and more weight to the sensing operation otherwise. Larger ρ value directly results in a more deterministic OTFS/OFDM symbol, while a smaller ρ results in a closer reference signal to a generic OTFS/OFDM frame consisting of randomly generated QPSK symbols. This reflects the deterministic-random tradeoff (DRT) in ISAC systems [3].

The scaling matrix $\boldsymbol{D}$ is defined in the subsection III-B where it is explained that D_{mn} scales the amplitude of the symbol in m-th subcarrier/delay bin and n-th time slot/Doppler bin proportionally to the radar cross section (RCS) of the target whose distance and velocity cause the time delay and Doppler shift values closest to the m-th delay bin and n-th Doppler bin. This keeps the symbol phase unchanged, which minimizes the hindrance to QPSK symbol detection. At the same time, symbols to be amplified are chosen specifically to represent the distance (time delay) and velocity (Doppler shift) of targets. Therefore, the synthesis of a precoded OTFS/OFDM symbol contains information about three different sensing parameters of a target in addition to its own communication message.

The precoded symbol vectors defined in section II can be determined optimally based on a reference signal, which is designed so that minimizing the difference to the reference signal will achieve the both goals of minimizing channel distortion and embedding the information regarding sensing targets into the transmit waveform. We write the following convex, bounded optimization problem:

$$\begin{aligned} \underset{\boldsymbol{x}}{min} \quad & ||\boldsymbol{H}_{eff}\boldsymbol{x} - \boldsymbol{s}_{ref}||_2, \\ \text{s.t.} \quad & ||\dot{\boldsymbol{x}}||_2^2 \leq P, \end{aligned} \tag{18}$$

where P is the total power constraint, $\boldsymbol{H}_{eff}$ is either $\boldsymbol{H}_{eff,OTFS}$ or $\boldsymbol{H}_{eff,OFDM}$ depending on the case, with $\dot{\boldsymbol{x}}$ being either $\dot{\boldsymbol{x}}_{OTFS}$ or $\dot{\boldsymbol{x}}_{OFDM}$ to match with it, and $\boldsymbol{s}_{ref} = \text{vec}(\boldsymbol{S}_{ref})$. Optimized vector $\boldsymbol{x}$ corresponds to the $\boldsymbol{x}_{DD}$ or $\boldsymbol{x}_{TF}$ expressions defined in Section II, and the CP-appended symbol vector $\dot{\boldsymbol{x}}$ will be defined in the subsection III-C for both cases. This optimization problem aims to have the receive processed symbol matrix $\boldsymbol{Y}$, which is equal to either $\text{vec}^{-1}(\boldsymbol{y}_{DD})$ or $\text{vec}^{-1}(\boldsymbol{y}_{TF})$, to have values with large magnitudes on the indices that correspond to the nonzero indices of $\boldsymbol{D}$, and otherwise contain values as close as possible to $\boldsymbol{S}$. A 2D constant false-alarm rate detector (CFAR) is then applied on $\boldsymbol{Y}$ to acquire the sensing data, before the communication symbol detection is done on $\boldsymbol{Y}$ as well.

B. Scaling matrix $\boldsymbol{D}$

A multiple path channel is defined in the DD domain in (2), with each path having time delay and Doppler shift effects on the signal that propagates through them. Likewise, sensing targets in the channel act as paths with signals echoing from them being subjected to their own time delay and Doppler shift. The paths that are caused by the channel environment and the sensing targets can be identified as $h_{DD,env}(\tau,\nu)$ and $h_{DD,tgt}(\tau,\nu)$, respectively. The detailed estimation of $h_{DD,env}(\tau,\nu)$ and $h_{DD,tgt}(\tau,\nu)$ is out of the scope of this paper. In practice, the CSI can be obtained via classic channel estimation or artificial intelligence (AI) based approaches. A discrete representation of $h_{DD,tgt}(\tau,\nu)$ would require a DD matrix of the same size as the symbol matrices $\boldsymbol{X}_{DD}$ and $\boldsymbol{X}_{TF}$. On an $M \times N$ grid that has M delay bins with $\frac{1}{M\Delta f}$ spacing and N Doppler bins with $\frac{1}{NT}$ spacing, Doppler shift at the n-th column is calculated as $\nu_n = \frac{n}{NT}$, while time delay at the m-th row is given by $\tau_m = \frac{m}{M\Delta f}$. For a target located at range x_k with velocity of v_k, its corresponding delay and Doppler offset in the given DD domain can be calculated as $\tau_k = \underset{\tau_m}{arg\,min}|\frac{2x_k}{c} - \tau_m|$, and $\nu_k = \underset{\nu_n}{arg\,min}|\frac{v_k}{\lambda} - \nu_n|$ respectively, where λ is the wavelength corresponding to the carrier frequency of the transmitted waveform. Delta functions in the definition of $h_{DD,tgt}(\tau,\nu)$ characterize the range and velocity of the target. The channel coefficient h_i for i-th path can be modeled as a factor related to the target RCS since channel paths of targets with low RCS will have a higher attenuation effect on the strength of the echoing signal and vice versa. We propose a scaling matrix $\boldsymbol{D} \in \mathbb{C}^{M\times N}$ so that for each target k, there is a nonzero element at the index D_{mn} defined as

$$D_{mn} = \begin{cases} c_k & \text{if } \tau_m = \tau_k \text{ and } \nu_n = \nu_k \text{ for any } k \in [1,K], \\ 0 & \text{otherwise,} \end{cases} \tag{19}$$

where $c_k \in [0,1]$ is the reflection factor of the target and is correlated with its RCS. Involving the representation of sensing target information (e.g. Doppler, distance and RCS) in the precoder design will lead to a waveform that is favorable for sensing while maintaining the communications performance.

C. Expressing the transmit signal with CP

While the input-output relations defined in (15) and (16) omit the representation of a CP-appended transmit signal due to the CP getting removed during receive processing, power constraint concerns the transmit signal exactly as it is and thus needs to be defined by the CP-appended transmit waveforms, $\dot{\boldsymbol{x}}_{OTFS}$ and $\dot{\boldsymbol{x}}_{OFDM}$. Reduced cyclic prefix (RCP) variant of the OTFS modulation is implemented in this work, in which the last l_{max} samples of $\boldsymbol{x}_{OTFS}$ are prepended to it. This can be achieved simultaneously with the transmitter processing when $\boldsymbol{x}_{OTFS}$ is multiplied with $(\boldsymbol{F}_N^H \otimes \boldsymbol{G}_{tx})$. Let us label the pre-CP transmit processing function as $\boldsymbol{T} = (\boldsymbol{F}_N^H \otimes \boldsymbol{G}_{tx})$. Expressing $\boldsymbol{T} \in \mathbb{C}^{MN\times MN}$ in terms of its $1 \times MN$ rows, we denote $\boldsymbol{T} = \left[\boldsymbol{T}_1^T, \boldsymbol{T}_2^T, \ldots, \boldsymbol{T}_{MN}^T\right]^T$, and in turn the post-CP transmit processing function $\dot{\boldsymbol{T}} \in \mathbb{C}^{(MN+l_{max})\times MN}$ is defined as $\dot{\boldsymbol{T}} = [\boldsymbol{T}_{MN-l_{max}+1}^T, \boldsymbol{T}_{MN-l_{max}+2}^T, \ldots, \boldsymbol{T}_{MN}^T, \boldsymbol{T}_1^T, \boldsymbol{T}_2^T, \ldots, \boldsymbol{T}_{MN}^T]^T$ The vector of transmitted RCP-OTFS samples can be written in terms of $\dot{\boldsymbol{T}}$ as $\dot{\boldsymbol{x}}_{OTFS} = \dot{\boldsymbol{T}}\boldsymbol{x}_{OTFS}$. In contrast to the OTFS case, OFDM signal requires CP for each time slot in the frame. Denoting the $\boldsymbol{X}_{OFDM}$ in terms of its $1 \times N$ row vectors as $\boldsymbol{X}_{OFDM} = \left[\boldsymbol{X}_1^T, \boldsymbol{X}_2^T, \ldots, \boldsymbol{X}_M^T\right]^T$, the CP-appended OFDM symbol matrix can be written as $\dot{\boldsymbol{X}}_{OFDM} = [\boldsymbol{X}_{M-l_{max}+1}^T, \boldsymbol{X}_{M-l_{max}+2}^T, \ldots, \boldsymbol{X}_M^T, \boldsymbol{X}_1^T, \boldsymbol{X}_2^T, \ldots, \boldsymbol{X}_M^T]^T$ Generating the $\text{vec}(\dot{\boldsymbol{X}}_{OFDM}) = \dot{\boldsymbol{x}}_{OFDM}$ directly is possible by defining a post-CP transmit processing function similarly to the OTFS case. Defining $\boldsymbol{f}_m$ as the m-th row vector of $\boldsymbol{F}_M^H$, we can write $\dot{\boldsymbol{F}}_M^H = \left[\boldsymbol{f}_{m-l_{max}+1}^T, \boldsymbol{f}_{m-l_{max}+2}^T, \ldots, \boldsymbol{f}_m^T, \boldsymbol{f}_1^T, \boldsymbol{f}_2^T, \ldots, \boldsymbol{f}_m^T\right]^T$ as and $\dot{\boldsymbol{x}}_{OFDM}$ can be written in terms of $\dot{\boldsymbol{F}}_M^H$ as $\dot{\boldsymbol{x}}_{OFDM} = (\boldsymbol{G}_{tx} \otimes \dot{\boldsymbol{F}}_M^H)\boldsymbol{x}_{OFDM}$. The expressions of $\dot{\boldsymbol{x}}_{OTFS}$ and $\dot{\boldsymbol{x}}_{OFDM}$ were used in Section III-A when defining the power constraint of (18) to portray the power distribution more accurately by considering the CP samples.

IV. Simulation results and analysis

A series of Monte Carlo simulations have been performed to acquire the average performance of the proposed precoding method with both OTFS and OFDM cases. The Extended Vehicular A (EVA) channel model [14] has been referred to set the power delay profile and time delays corresponding to channel taps. Doppler shifts for the channel taps were randomized according to the Jakes' power spectrum model. The sensing targets were simulated by defining additional channel paths by using the methods in [12] where a time domain channel matrix is defined from time delay, Doppler shift, and path gain parameters, which are generated analogously as range, velocity, and reflection factor values in our simulation, respectively. A total of 30 targets were generated this way and their parameters were used in creating the effective channel matrix. M and N dimensions were both set as 64, bandwidth was set as 1 MHz, carrier frequency was set as 10 GHz, and maximum expected UE velocity was assumed to be 120 km/h. The power budget P was set to 70 dBm, with a 30 dBm transmitting power amplifier output and 20 dBi gain on both the transmitting and receiving antennas. Assuming -90 dBm receiver sensitivity (noise floor) and 30 dB total processing loss, there will still be 100 dB (SNR = 30 dB) to 130 dB (SNR = 0 dB) reserved for path loss. This power budget yields a 0.24$\sim$7.5 km coverage in free-space propagation and still spans a comparable coverage area, even considering atmospheric attenuation. A range of ρ values were used in evaluating different iterations of the simulation to observe the effect of weight allocation on either of the operations. MATLAB package CVX was used for solving the optimization problems [15]. The tradeoff between communication and radar performance is evaluated by P_d of the sensing targets, which is calculated by the ratio of successfully detected targets to the total number of targets, and by bit error rate (BER) of the communication operation. False alarm rate threshold of the CFAR detector was set to 0.01 for the simulations.

It can be observed in Fig. 2 that communication performance deteriorates more severely in the OTFS case when more weight is allocated to increase the P_d. This situation can be

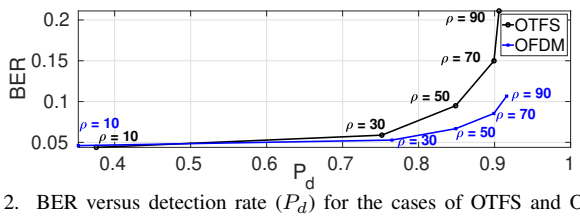

Fig. 2. BER versus detection rate (P_d) for the cases of OTFS and OFDM modulations, with varying ρ values, and SNR $= 5$ dB.

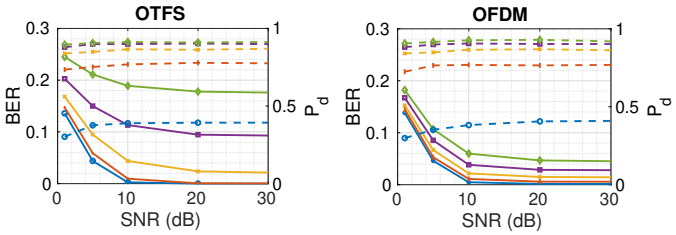

Fig. 3. BER (solid lines) versus SNR is plotted with straight lines while P_d (dash lines) versus SNR is plotted with dashed lines for the cases of OTFS and OFDM modulations precoded with varying ρ values, represented with following markers: $\circ$ $\rho = 10$, | $\rho = 30$, $\times$ $\rho = 50$, $\blacksquare$ $\rho = 70$, $\blacklozenge$ $\rho = 90$

observed more clearly in Fig. 3 where the changes in BER for varying SNR values are shown. Detection rate with respect to different SNR values can be observed from the same figure, where the P_d values increase with the SNR until they approach a ceiling around $P_d \approx 0.9$, which can be attributed to some of the targets having too low reflectivity factors to the point that the 2D CFAR detector cannot distinguish their cells from the cells that contain the QPSK symbols.

The key observation to be made from Fig. 2 and Fig. 3 is that system performance is comparable between the OTFS and OFDM systems in most cases, except when $\rho > 50$, in which case the communication performance is heavily compromised in the OTFS case as BER floor increases to the point that it is unrecoverable even with channel coding techniques. This could be interpreted as a consequence of the OTFS modulation spreading the communication message over a longer frame of length MN while OFDM frames are of length M. The transmit function for the OFDM is $\boldsymbol{G}_{tx} \otimes \boldsymbol{F}_M^H$, which is a matrix that contains copies of $\boldsymbol{F}_M^H$ on its diagonal, while the OTFS transmit function $\boldsymbol{F}_N^H \otimes \boldsymbol{G}_{tx}$ has its nonzero values spread more unevenly along the whole matrix.

Consequently, nonzero values of $\boldsymbol{H}_{eff,OFDM}$ are concentrated closer to the diagonal compared to $\boldsymbol{H}_{eff,OTFS}$. This situation reduces the degrees of freedom when optimizing an OTFS waveform to be as close as possible to $\boldsymbol{s}_{ref}$ while including larger values in indices that correspond to sensing target cells. This phenomenon is presented visually in Fig. 4 where it can be observed that producing $\boldsymbol{s}_{ref}$ as a result of $\boldsymbol{H}_{eff}\boldsymbol{x}$ is a more restricted task when the effective channel is defined for the OTFS case and ρ is higher.

V. Conclusion

In this work, we proposed a reference signal-based precoding method that reshapes the communications waveform to make it more favorable for performing sensing functions. The proposed precoding scheme is applicable to either OFDM or OTFS signals, which are widely adopted and tested in the 5G

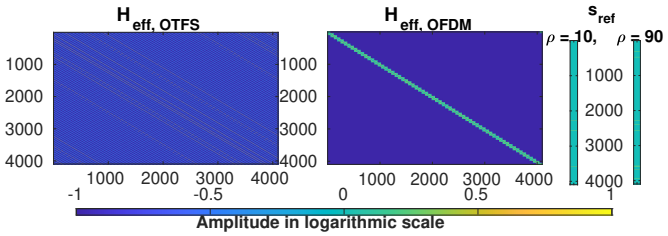

Fig. 4. Effective time domain channels for the OFDM and OTFS cases, along with the visualization of the reference signal amplitudes in $\rho = 10$ and $\rho = 90$ cases.

and perspective 6G systems. The comparative study and simulation results showed that the OFDM signal demonstrates more robustness in maintaining the communications performance (in terms of BER) when the signal is reshaped for sensing. In our future work, we will enhance the ISAC waveform design with AI. The benefit of embedding AI in ISAC waveform design can be embodied in two folds: i). Development of neural network model as an AI-based alternation to the convex optimization approach for solving (18) in Section III-A; ii). A more accurate channel state information model is used for scaling matrix design in Section III-B.

References

[1] J. A. Zhang et al., "Enabling Joint Communication and Radar Sensing in Mobile Networks—A Survey," in *IEEE Communications Surveys & Tutorials*, vol. 24, no. 1, pp. 306-345, Firstquarter 2022.

[2] N. González-Prelcic et al., "The Integrated Sensing and Communication Revolution for 6G: Vision, Techniques, and Applications," in *Proceedings of the IEEE*, vol. 112, no. 7, pp. 676-723, July 2024.

[3] Y. Xiong, et al., "On the Fundamental Tradeoff of Integrated Sensing and Communications Under Gaussian Channels," in *IEEE Transactions on Information Theory*, vol. 69, no. 9, pp. 5723-5751, Sept. 2023.

[4] J. A. Zhang, et al., "Multibeam for Joint Communication and Radar Sensing Using Steerable Analog Antenna Arrays," in *IEEE Transactions on Vehicular Technology*, vol. 68, no. 1, pp. 671-685, Jan. 2019.

[5] C. D. Ozkaptan, et al., "OFDM Pilot-Based Radar for Joint Vehicular Communication and Radar Systems," 2018 IEEE Vehicular Networking Conference (VNC), Taipei, Taiwan, Dec. 2018, pp. 1-8.

[6] A. Göktas, M. Ashraf, M. Valkama and B. Tan, "Optimal Joint Radar and Communications Beamforming for the Low-Altitude Airborne Vehicles in SAGIN," 2023 *IEEE WCNC*, Glasgow, United Kingdom, 2023, pp. 1-5

[7] M. F. Keskin, et al., "Integrated Sensing and Communications With MIMO-OTFS: ISI/ICI Exploitation and Delay-Doppler Multiplexing," in *IEEE Transactions on Wireless Communications*, vol. 23, no. 8, pp. 10229-10246, Aug. 2024.

[8] P. Raviteja, et al., "Embedded Delay-Doppler Channel Estimation for Orthogonal Time Frequency Space Modulation," *2018 IEEE 88th Vehicular Technology Conference*, Chicago, IL, USA, 2018, pp. 1-5.

[9] Y. Ge, Q. Deng, P. C. Ching and Z. Ding, "Receiver Design for OTFS with a Fractionally Spaced Sampling Approach," in *IEEE Transactions on Wireless Communications*, vol. 20, no. 7, pp. 4072-4086, July 2021.

[10] O. Zacharia and M. Vani Devi, "Fractional Delay and Doppler Estimation for OTFS Based ISAC Systems," *2023 IEEE WCNC*, Glasgow, United Kingdom, 2023, pp. 1-6

[11] T. Thaj and E. Viterbo, "Low Complexity Iterative Rake Decision Feedback Equalizer for Zero-Padded OTFS Systems," in *IEEE Transactions on Vehicular Technology*, vol. 69, no. 12, pp. 15606-15622, Dec. 2020.

[12] P. Raviteja, Y. Hong, E. Viterbo and E. Biglieri, "Practical Pulse-Shaping Waveforms for Reduced-Cyclic-Prefix OTFS," in *IEEE Transactions on Vehicular Technology*, vol. 68, no. 1, pp. 957-961, Jan. 2019.

[13] F. Liu, et al., "Toward Dual-functional Radar-Communication Systems: Optimal Waveform Design," in *IEEE Transactions on Signal Processing*, vol. 66, no. 16, pp. 4264-4279, Aug. 2018.

[14] 3GPP TS 36.104. "LTE; E-UTRA; BS radio transmission and reception (Release 14)" *3rd Generation Partnership Project; Technical Specification Group Radio Access Network.*

[15] CVX Research, Inc. CVX: Matlab software for disciplined convex programming, version 2.0. https://cvxr.com/cvx, April 2011.